Article:
Soto-Alvarez, M, Alcayaga, H, Alarcon, V et al. (2020) Evaluation of products 3B42 v7 and 3IMERG for the hydroclimatic regions of Chile. Journal of South American Earth Sciences, 104. 102870. ISSN: 0895-9811

https://doi.org/10.1016/j.jsames.2020.102870

Journal of South American Earth Sciences 104 (2020) 102870

Contents lists available at ScienceDirect

Journal of South American Earth Sciences

journal homepage: www.elsevier.com/locate/jsames

Evaluation of products 3B42 v7 and 3IMERG for the hydroclimatic regions of Chile

Marco Soto-Alvarez [a,*], Hernán Alcayaga [a], Vladimir Alarcon [a], Diego Caamaño [b], Sebastián Palma [a], Rossana Escanilla [a]

[a] Dept. of Engineering and Sciences, Universidad Diego Portales, Av. Ejército 441, Santiago, 8370109, Chile
[b] Dept. of Civil Engineering, Universidad Católica de la Santísima Concepción, Campus San Andrés, Alonso Ribera 2850, Concepción, 4030000, Chile

ARTICLE INFO

Keywords:
Rainfall
TRMM
GPM
Hydroclimatic zones

ABSTRACT

Data provided by products 3B42 V7 (TRMM) and its successor 3IMERG (GPM) are compared with discrete rainfall information throughout the Chilean territory covering four macro hydroclimatic zones. Precipitation data was obtained from weather stations available on a daily basis from the 1930s to present. A total of 143 stations were chosen and rainfall estimates performed for years 2014 through 2018. Applying the same metrics we showed how GPM performances improve as the temporal aggregation increases. Several drawbacks were detected in the coastal areas, which were characterized by lower accuracy performances than internal areas. However, the 3IMERG product could be a strong source of data to study the impact that climatic disturbances have on the hydrologic cycle in the Central and South zones of Chile. Additionally, its offers a fundamental source of data for remote zones or areas where access is complicated to install weather stations.

1. Introduction

In recent years Chile has experienced a constant economic growth (OECD, 2018), having water resources play a fundamental role in several economic activities responsible for such trend. Therefore, in order to maintain a sustainable development, an appropriate water management is required. Proper performance of this task is highly related to the quantity and quality of water data in order to have a good spatial and temporal representation. This presents a challenge in Chile because of its extreme climate variability and complex geography (McPhee, 2018). Thus, the local water agency is continuously struggling maintaining monitoring stations and installing new ones in remote areas. Nowadays, satellite-based rainfall estimates (SRE's) offer a good alternative to improved data availability (Blöschl et al., 2019), and these new tools require an assessment upon the particular Chilean conditions.

SRE's have been widely used around the world (Cao et al., 2018; Dinku et al., 2007) to generate useful rainfall data. The evolution of SRE's allowed for the generation of rainfall estimates with increasing temporal and spatial resolution. However, Tian et al. (2009), Alarcon et al. (2015) and Zambrano-Bigiarini et al. (2017), report these estimates still introduce uncertainties when data are used for hydrological research. Efforts have been made to validate and calibrate these products in different parts of the world (e.g. Bharti and Singh, 2015; Cabrera et al., 2016; Caracciolo et al., 2018; Dinku et al., 2007; Dinku et al., 2008; Rivera et al., 2018; Sharifi et al., 2016; Tan and Santo, 2018; Tarek et al., 2017; Wang et al., 2017; Zad et al., 2018) and also in Chile (e.g. Baez-Villanueva et al., 2018; Demaria et al., 2013; Hobouchian et al., 2017; Mendez Rivas, 2016; Zambrano-Bigiarini et al., 2017). Results showed to be strongly sensitive to topography and rainfall seasonality (Hobouchian et al., 2017; Mendez Rivas, 2016; Zambrano-Bigiarini et al., 2017), as well as the spatial and temporal resolution of the products (e.g. Baez-Villanueva et al., 2018; Tan and Santo, 2018). Particularly in Chile, factors such as topography, snow, wind and types of cloud cover affect not only field data collection but also SRE's (World Meteorological Organization -WMO, 2014; Zambrano-Bigiarini et al., 2017). In northern Chile, latitudes 17° 29′S and 25°S, the strongest rainfall events occur during summer and mostly in the highlands (Houston, 2006). In Central and Southern Chile, cyclonic precipitation events are conditioned by the Pacific Ocean's atmospheric activity (Barrett and Hameed, 2017). In addition, due to the country's rugged topography (it is located between two mountain ranges, Cordillera de Los Andes and Cordillera de La Costa), convective and orographic precipitation, as snowfall in the highlands are important (e.g. Garreaud et al., 2016; Houston, 2006; Insel et al., 2010).

* Corresponding author.
E-mail address: marcosoto.al@gmail.com (M. Soto-Alvarez).

https://doi.org/10.1016/j.jsames.2020.102870
Received 25 April 2020; Received in revised form 15 August 2020; Accepted 30 August 2020
Available online 3 September 2020

Recent studies Baez-Villanueva et al. (2018), Hobouchian et al. (2017), Mendez Rivas (2016), and Zambrano-Bigiarini et al. (2017) have shown that the Tropical Rainfall Measuring Mission (TRMM) with 3B42 V7 product provides the best results for its spatial (0.25 ° × 0.25 ° lat/lon) and temporal (every 3 h) resolution on specific macro zones or basins in the Chilean territory. Rainfall estimates from the Global Precipitation Mission (GPM) with 3IMERG (Level-3 Integrated Multi-satellite Retrievals) product has not been widely assessed for its use in Chilean territory. Tan and Santo (2018), in a study carried out in Malaysia, concluded that the IMERG product's estimations compared better to ground station rainfall data than other SRE's such as PERSIANN-CDR and its predecessor 3B42 V7.

There is a need to evaluate the SRE's performances in more variable spatial and temporal scales, to cover different climate and geographic areas of Chile. The aim of this paper is to assess the data provided by products 3B42 V7 (TRMM) and its successor 3IMERG (GPM) throughout the country and thus covering several macro hydroclimatic zones of Chile. The assessment is performed for rainfall estimates for years 2014 through 2018.

2. Data and methods

2.1. Study area and macro hydroclimatic zones

The area covered by this study corresponds to continental Chilean territory (South America), between latitudes ~17° S and ~56° S, and longitudes ~76°W and ~66°W (Fig. 1). Its latitudinal extent of around 4300 km, gives Chile diverse climatic characteristics. According to McPhee (2018), the territory can be separated into different macro zones associated with distinct hydrological regimes. The macro zones used in this study, as defined by McPhee (2018), are: North, Central, South and Austral (Fig. 1).

The North macro zone corresponds to the Atacama Desert basins. These are characterized by extreme arid conditions imposed by the Pacific Anticyclone, which hinders the entry of humid air masses from the southwest. In addition, the Andes Mountain Range obstructs the entry of air masses with high moisture content from the East. For these reasons, the plains of the interior of the Atacama Desert are considered the driest areas of the planet; for example, in Quillagua rainfall station the average measured annual rainfall is 0.15 mm. Much of the precipitation occurs in high altitude areas (over 2000 m.a.s.l, called *Altiplano*)

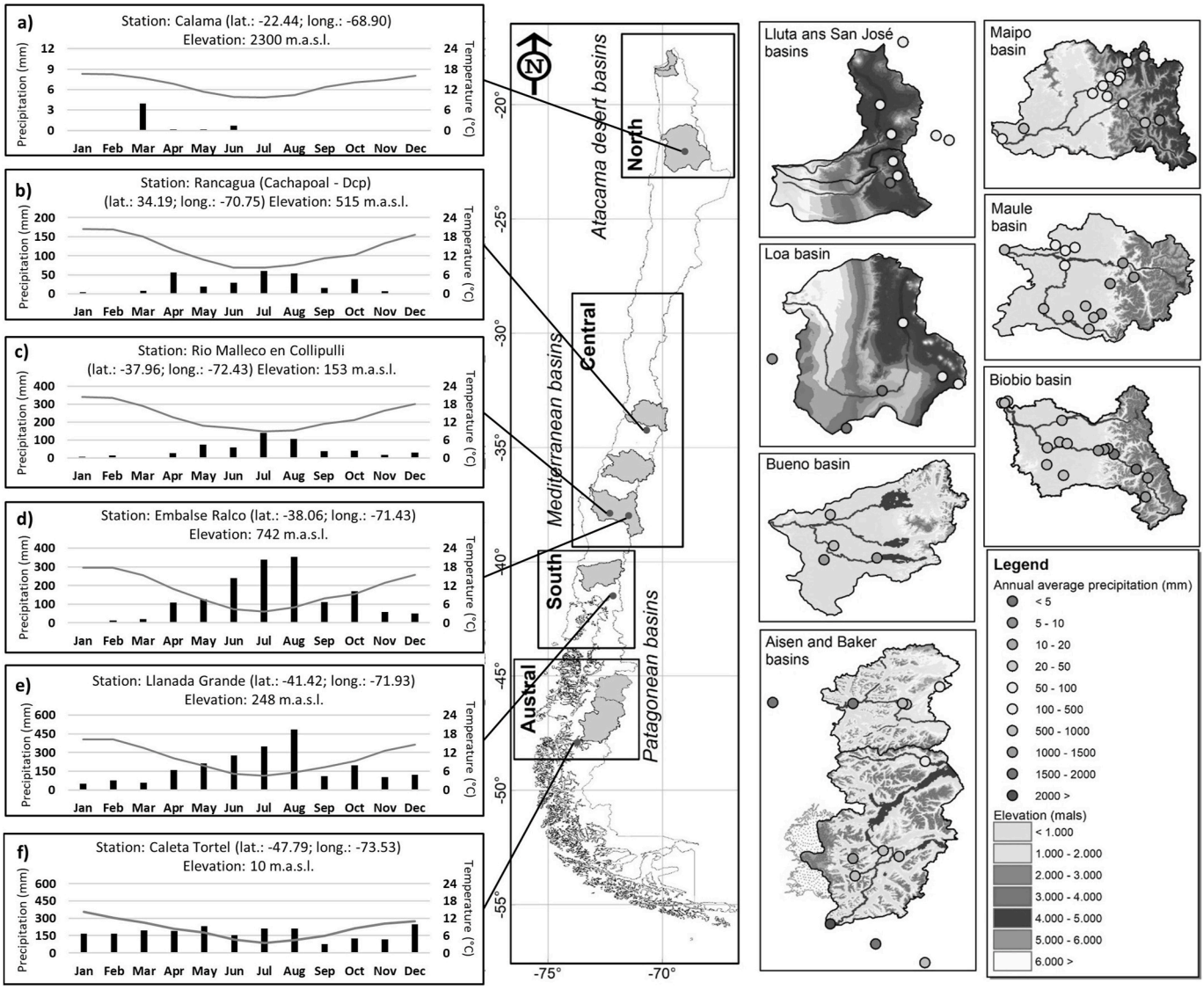

Fig. 1. Study area and macro hydroclimatic zones defined by its hydrological, climate and topographical characteristics. The hyetographs from a) to f) correspond to the average monthly precipitation from representative weather stations of each macro hydroclimatic zone. The circle colors represent the range of annual average precipitation (mm) for each meteorological station analyzed.

during the months of January to March, and precipitation above 4000 m.a.s.l. generally corresponds to snow (Houston, 2006).

Precipitation in the Central macro zone is also under the influence of the Pacific Anticyclone, which moves northward during fall (March, April, May), during winter (June, July, August) and spring (September, October, November), when the most intense precipitation events occur (Barrett and Hameed, 2017). The Central macro zone has the characteristics of Mediterranean climates, with precipitation concentrated between June and September. This zone includes the Coastal Mountain Range, which together with the Andes Mountain Range, represent the two most important geographic factors for the occurrence of precipitation (Garreaud et al., 2016; Insel et al., 2010), which comes in the form of rainfall (in a large part of this territory) and snow (over 2000 m.a.s.l). In this macro zone the precipitation gradients are very high: for example, in the southern Biobio basin average annual precipitation increases from 579.03 mm (Río Malleco Station) to 1388.48 mm (Embalse el Ralco Station) in a distance of 88 km (See Fig. 1). This orographic component is generated in a firstly by the clash between the Pacific Ocean frontal system and the Coastal Mountain Range. Later, the phenomenon of elevation and cooling of the air masses is further intensified when air and humidity reach the Andes Mountain Range (some mountain peaks are above the 5000 m.a.s.l.)

In the Southern and Austral macro zones, precipitation is characterized by intense rainfall and snow events and lower temperatures. On the one hand, the Southern macro zone has the highest annual rainfall in the country, for example the precipitation could reach up to 7330 mm per year in the Guarello station (Gunn, 2004). On the other hand, the Austral macro zone differs from the Southern macro zone with its low temperatures and the more moderate amounts of precipitation, which occur throughout the year (McPhee, 2018). The Austral macro zone is conditioned by cold masses coming from Antarctica region that influence the type of precipitation, causing the fall and accumulation of snow.

2.2. Meteorological stations

Precipitation data was obtained from weather stations available through the Center for Climate and Resilience Research (www.cr2.cl). The downloaded database contains daily information from the 1930s to present. Some meteorological stations showed important gaps in information, thus 17% (143 stations) of the total available stations were used. The selected stations had records with at least 90% availability of data, using data from March-12-2014 through March-09-2018.

2.3. Satellite-based rainfall estimates

Satellite-based rainfall estimates (SRE's) data from March 2014 to March 2018 was downloaded from the NASA website Goddard Earth Sciences Data and Information Services Center (GES-DISC) (disc.gsfc.nasa.gov). This center archives information used to study the atmosphere, water, energy and climate change. The products are available for download in NetCDF format, including a significant portion of the planet that considers the Chilean territory. The next items describe the calibration-based sequential scheme Multisatellite Precipitation Analysis (TMPA), and the Integrated Multi-satellite Retrievals for GPM (IMERG) project detailing the products and equipment used for producing the precipitation estimations.

2.3.1. TRMM Multisatellite Precipitation Analysis (TMPA)

Using the information obtained by the TRMM (until stopped collecting data in April 2015), the TMPA scheme calibrates the rainfall estimates using the information provided by satellites equipped with passive microwave measurement sensors (PMW), infra-red geostationary information (IR) (Kidd and Levizzani, 2011). Also, the satellite data is adjusted with ground precipitation data from the World Precipitation Climatology Center (GPCC) and the monthly precipitation analysis from the Climate Assessment and Monitoring System (CAMS) developed by the Climate Prediction Center (CPC) (Huffman et al., 2007). The products of this calibration-based scheme are 3B42 and 3B43. TRMM 3B42 data is provided with a spatial resolution of $0.25^\circ \times 0.25^\circ$, between latitudes 50° north and south; and temporal resolution of 3 h. TRMM 3B43 products are similar datasets but with a monthly resolution (Huffman, 2016). In addition, the TMPA products are provided in real time and post-real time. The first has a processing time of 8–9 h, while the second has 2.5 months after of the month's end (Huffman, 2016; Huffman et al., 2007). Both products are calculated using the Goddard profiling algorithm used by the TMPA (32), however, the real time products (3B40RT/3B41RT/3B42RT), unlike the real time post (3B42/3B43), are calibrated with climatological factors data (Huffman et al., 2010).

2.3.2. Integrated Multi-satellite retrievals for GPM (IMERG)

The GPM joint international project using data from satellites equipped with microwave sensors (JAXA, 2018) and the inclusion of the Dual-frequency Precipitation Radar (DPR) and GPM microwave imager (GMI). The NASA (USA) and JAXA (Japan) mission commenced collecting data on February 28, 2014, covering a scanning area between latitudes 60° North and 60° South. The DPR and GMI equipment replace the Precipitation Radar (PR) and TRMM Microwave Imager (TMI), respectively. The DPR has dual frequency radars of Ku (13.6 GHz) and Ka (35.55 GHz) bands, unlike the PR which had one frequency radar of ~13.8 GHz. The Ku precipitation radar (KuPR) is capable of identifying the most intense precipitations (>0.5 mm/h), while the KaPR precipitation radar is capable of identifying lighter precipitations (>0.2 mm/h). The IMERG system delivers two products in real time, the Early and Late version, and one product in post time, called Final Run. The latter can be downloaded with half-hour (3IMERGHH) and monthly (3IMERGM) temporal resolution. The Early product (3IMERGHH-E) and Late product (3IMERGHH-L) are uploaded to the system after 4–6 and 12–18 h, respectively, after data collection. In contrast, the Final Run versions 3IMERGHH and 3IMERGM are delivered 3 months after data collection (Huffman et al., 2017). The product of the 3IMERG data is provided with a spatial resolution of $0.1^\circ \times 0.1^\circ$, between latitudes 60° north and south.

The satellite-based rainfall estimates used in this paper are the final versions of TMPA and IMERG: 3B42 V7 and 3IMERGHH (hereafter called 3IMERG), respectively. The data spatial coverage ranges from latitude 17°S to latitude 50°S, the latter corresponding to the maximum coverage of TMPA data. In addition, the data spatial-resolution for each product (Fig. 2) was not modified to be able to capture precipitation estimates in sectors with steep slopes. Daily 3B42 V7 and 3IMERG rainfall estimates were assessed in this research.

2.4. Data comparison

The daily data collected by meteorological stations (observed daily depth rainfall, O) were compared seasonally to 3IMERG and 3B42 V7 (estimated depth rainfall, E) using two different types of statistical indices indicated as categorical and continuous. As stated above, the spatial resolution of each product was not modified; finer spatial resolutions (3IMERG product) allowed assessing rainfall estimates in areas with high elevation gradients. Topographical elevation zones were classified as follows: low (<1000 m.a.s.l.), medium (between 1000 and 2000 m.a.s.l.), and high (>2000 m.a.s.l.).

The categorical statistical indices quantify the ability of SRE's to identify the occurrence and non-occurrence of precipitation events in a per day basis. The categorical variables used to calculate those indices were, Hit (or Success, H), False Alarm (FA), Missing value (M) and a Correct Negative (CN). If a precipitation event occurred on any day and the satellite correctly identified the event, that day counts as a success (H). If the event was observed at the station and was not identified by the remote sensor, that day is categorized as a Missing value (M). When the

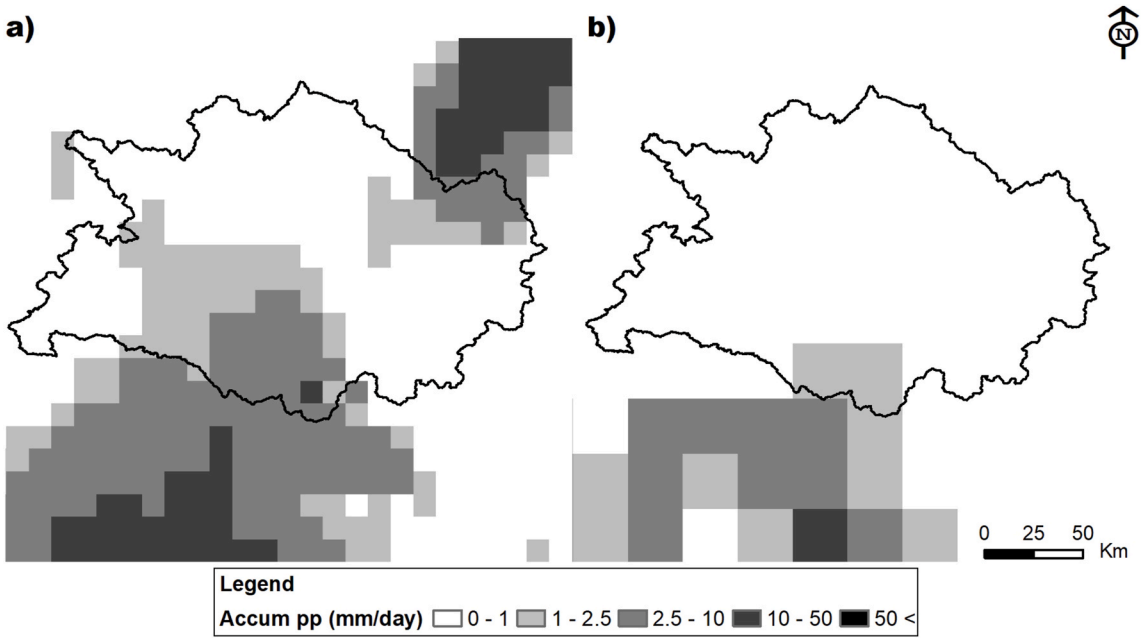

Fig. 2. Spatial resolution of a) 3B42 V7 and b) 3IMERG products. Both Fig. 2a and b representing daily accumulated precipitation (Accum pp) for the rainfall event of July 18th, 2015 in the río Maule watershed (Central macro zone).

SRE's identifies the occurrence of an event that has not been observed on the ground, that day is categorized as False Alarm (FA). When a precipitation event has not been estimated nor observed, it is categorized as a Correct Negative (CN).

The Percentage of Correct estimates index PC (Equation (1)) is the fraction of correctly identified events (H + CN) over the total number of days analyzed (N_e). The Probability Of Detection index, POD (Equation (2)), is the ratio of successfully identified events to total events occurred (H + M). The False Alarm Ratio, FAR (Equation (3)), is the total number of false alarms divided by the total number of precipitation events identified by the satellite (H + FA). The equitable threat score, ETS (Equation (4)), is the ratio of successfully identified events to total estimated and observed events (H + FA + M), adjusted by the frequency of randomly estimated events, He (Equation (5)) (Gupta et al., 2009; Kling et al., 2012; Zambrano-Bigiarini et al., 2017). The ranges (minimal and maximal) and the optimal values for these four categorical indices are presented in Table 1.

$$PC = \frac{H + CN}{N_e} \tag{1}$$

$$POD = \frac{H}{H + M} \tag{2}$$

$$FAR = \frac{FA}{H + FA} \tag{3}$$

Table 1
Minimal (Min), maximal (Max) and optimal values for categorical and continuous indices.

Index type	Index name	Min	Max	Optimal
Categorical	PC	0	1	1
	POD	0	1	1
	FAR	0	1	0
	ETS	−1/3	1	1
Continuous	R	−1	1	1
	BIAS	-∞	+∞	1
	KGE′	-∞	1	1
	Γ	-∞	+∞	1

$$ETS = \frac{H - H_e}{(H + FA + M) + H_e} \tag{4}$$

$$H_e = \frac{(H + M)^*(H + FA)}{N_e} \tag{5}$$

Continuous statistical indices measure the error of i) precipitation estimates temporal dynamics, ii) bias (overestimation or underestimation), and iii) the variability of the estimated rainfall magnitude. For the study of hydrological models, numerous criteria have been used to indicate the fit between observed and estimated data. Based on Gupta et al. (2009) and Kling et al. (2012) this research uses the modified Kling-Gupta efficiency (KGE′) method of measuring estimated vs observed rainfall data fit, (Equation (6)). The KGE′ uses a combination of the linear correlation coefficient, r (Equation (7)), the BIAS, (Equation (8)), and the variability ratio, γ (Equation (9)) to assess the quality of the SRE's data.

$$KGE^{'} = 1 - \sqrt{(r-1)^2 + (BIAS-1)^2 + (\gamma-1)^2}, \tag{6}$$

$$r = \frac{\sum_{i=1}^{n}\left(O_i - \overline{O}\right)^*\left(E_i - \overline{E}\right)}{\sqrt{\sum_{i=1}^{n}\left(O_i - \overline{O}\right)^2}^*\sqrt{\sum_{i=1}^{n}\left(E_i - \overline{E}\right)^2}} \tag{7}$$

$$BIAS = \frac{\mu_E}{\mu_O} \tag{8}$$

$$\gamma = \frac{\sigma_E/\mu_E}{\sigma_O/\mu_O} \tag{9}$$

where O_i is the i observed data, E_i is the i estimated data from the SRE's, σ_E and σ_O are the standard deviation of the estimated and observed values, μ_E and μ_O' are the average of all estimated and observed values, respectively. The ranges (minimal and maximal) and the optimal values for these four continuous indices are presented in Table 1.

3. Results

The results are presented first for the categorical indices and then for

the continuous indices, which were calculated for the entire study period (March 2014 to March 2018). For both products 3IMERG and 3B42 V7, the results showed differences that depend on the macro zone and the season of the year.

3.1. Detection index

The annual inter seasonality of the rainfall regime affects the performance of the SRE's. This is reflected in the results of the detection indices for each season of the year. These results are presented in Fig. 3.

The values of the PC indicator show a high probability of event identification for each product (PC > 0.5 for all seasons and macro zones), where the 3IMERG has greater probabilities to correctly detect than 3B42 V7. For the **North macro zone** and during the summer (called Altiplano winter), the 3IMERG reaches a maximum PC of 0.79, this value corresponds to the lowest value obtained with respect to the other seasons of the year. The maximum PC value in the North macro zone during the winter months was 0.94. The 3B42 V7 product obtained an average PC of 0.83 in the summer months, this last value being the highest obtained by this product in the North macro zone. In the **Central macro zone**, the best values for the PC indicator, in this case of 3IMERG and of 3B42 V7 were found in the summer months, with a maximum PC of 0.83 and 0.88 respectively. The lowest PC values of all the analysis were obtained in the **South and Austral macro zones** (see Fig. 3). Of these values, the 3IMERG product has a minimum PC of 0.72 (South) and 0.67 (Austral) during the spring months. The 3B42 V7 has a minimum PC of 0.55 (for both macro zones) during the winter months.

According to the POD indicator both products are good detecting rain events. In the North macro zone the highest POD values were found in the summer months, in this season the 3IMERG and 3B42 V7 products presented a maximum POD of 0.84 and 0.64, respectively (these are the highest of all the macro zones). The Central, South and Austral macro zones have results similar throughout the entire year. For these three macro zones (Central, South and Austral), the product 3IMERG reaches a maximum POD of 0.75, 0.79 and 0.73, while for the 3B42 V7 the maximum POD is 0.42, 0.43 and 0.37, respectively. All the maximum POD values mentioned previously are obtained between the autumn and winter seasons.

The results of the false alarm ratio index (FAR), as with the case of the two previous indices (PC and POD), present the best results for the North macro zone during the Altiplano winter. The 3IMERG has a higher FAR index than the 3B42 V7, therefore, in this macro zone the 3B42 V7 offers a lower quantity of false alarms. However, this condition is reversed during the autumn, winter and spring seasons where the performance of the 3IMERG is better than the 3B42 V7 (for these three seasons the average FAR was of 0.80 for the 3IMERG and 0.87 for the 3B42 V7). As with the North macro zone, in the Central, South and Austral macro zones the 3IMERG product obtains a greater FAR (average FAR of 0.39) than the 3B24 V7 product (average FAR of 0.32).

From the ETS indicator results, it was evidenced that the values are greater than zero, however, they don't have the ability to capture the fraction of rain events correctly (in general, for both SRE's the ETS was less than 0.33 in all the macro zones and seasons of the year). In the North macro zone, during the summer months the ETS value was 0.33 for both products, this value corresponds to the maximum obtained for the macro zones and the seasons of the year. In the Central macro zone the highest ETS values were in the autumn and winter seasons. In this same macro zone the 3IMERG product obtains for the winter season an average ETS of 0.24, while the 3B42 V7 product obtains for the autumn season an average ETS of 0.21. In the South macro zone the 3IMERG product concentrates the best results during the dry season (spring and summer) with a maximum ETS of 0.29 (spring). For this same macro zone, the best results for the 3B42 product is a maximum ETS of 0.16 (autumn). Finally, in the Austral macro zone the best results for the ETS indicator, for both products, was during the summer and autumn months. The maximum ETS values for the 3IMERG product was 0.28 (summer), while the maximum ETS values for the 3B42 V7 product was 0.15 (autumn).

According to the results of Fig. 3, the North macro zone has a marked influence of the seasons on the POD, FAR and ETS values. For both products, the best performance is associated with greater amounts of rain during the Altiplano winter (in summer). The same performance condition of the SRE's is present in the Central and South macro zones. These two macro zones are characterized by a Mediterranean climate, where the majority of the rain concentration occurs between the autumn and spring seasons (see Fig. 1).

The high averages for the POD and FAR obtained in the macro North zone in this study (3IMERG, POD = 0.60 and FAR = 0.72; 3B42 V7, POD = 0.56 and FAR = 0.75) are consistent with the observed by Mantas et al. (2014), in the south zone of Peru for the 3B42 V7 product (average POD and FAR of 0.60 and 0.57, respectively). In the Central macro zone, the POD and FAR indices obtained in this study in wet seasons (3IMERG,

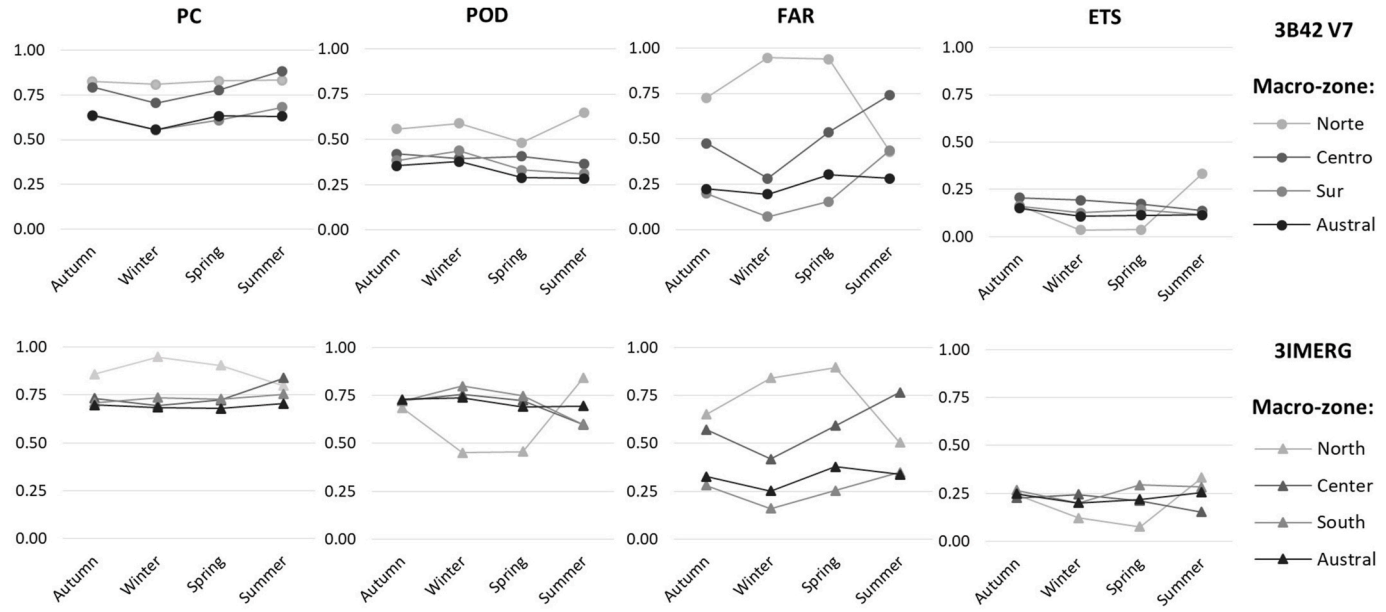

Fig. 3. Detection indices (PC, POD, FAR, and ETS) for each macro zones per seasons; Summer, (DJF), Autumn (MAM), Winter (JJA) and Spring (SON).

POD = 0.73 and FAR = 0.49; 3B42 V7, POD = 0.40 and FAR = 0.37) are better than those obtained in the dry seasons (3IMERG, POD = 0.66 and FAR = 0.67; 3B42 V7, POD = 0.38 and FAR = 0.63). The good POD results for the dry seasons were in the central zone of Chile obtained by Hobouchian et al. (2017). Thus, it was obtained an average POD of 0.97 (3IMERG) and 1.00 (3B42 V7) for the wet seasons and the average POD of 0.71 (3IMERG) and 0.66 (3B42 V7) for the dry seasons. In contrast, the FAR results for 3IMERG do not show variation (FAR = 0.25) between the seasons, while the 3B42 V7 showed a worse performance in the wet season (FAR = 0.39) than in the dry season (FAR = 0.18).

Comparing the average ETS index results calculated in this study for the central macro zone (3IMERG, ETS = 0.23 and 3B42 V7, ETS = 0.14), with those obtained by Zambrano-Bigiarini et al. (2017; 3B42 V7, ETS<0.2) and Rivera et al. (2018; 3B42 V7, ETS = 0.23) it was found that the 3IMERG results do not show an improvement in the detection abilities of events and that the 3B42 V7 is even under the values cited before.

Next, an analysis is performed on the detection indices for each of the basins defined in this study. This analysis is presented in Fig. 4, for the PC and POD indices. Following which, in Fig. 5 the results for the FAR and ETS index analysis is presented.

In general the 3IMERG product, with an average PC = 0.75, is under the 3B42 V7, which obtained an average PC = 0.82. The good results of the 3B42 V7 product according to the PC indicator is due to the overestimation of events by the 3IMERG product, and the lower quantity of correct negatives that the latter one obtained.

The POD indicator has the best results for the 3IMERG product in the Maipo basin (Central macro zone), with an average POD of 0.85 and a maximum POD of = 0.96. This same product obtained similar average values in the other basins analyzed (mean POD in a range of 0.80–0.90), with exception the Loa basin, where the mean POD = 0.55. On the other hand, the 3B42 V7 obtains its best performance in the Lluta and San José basins (macro North zone), with an average POD of 0.71 and a maximum POD = 0.86. The POD results for the other basics were within the range 0.38–0.57.

The results for each basin for the FAR index are presented in Fig. 5. The best results for this index were obtained in the Río Bueno basin (South macro zone) for both the 3IMERG (mean FAR 0.36) and the 3B42 V7 (mean FAR 0.28). In contrast, in the basins located in the north macro zone (Río San José, Lluta and Loa basins) both products, 3IMERG and 3B42 V7, obtain the worst results (see Fig. 5).

In the same Fig. 5 we can see the evaluation of both products through the ETS index. This analysis verified that the event detection efficiency for the 3IMERG is better than the 3B42 V7 (mean ETS for 3IMERG and the 3B42 V7 is 0.25 and 0.18, respectively). However, the results indicate that both satellite products do achieve a satisfactory identification of the precipitation events, having a high probability of success due to coincidence.

3.2. Continuous indices

The results for the Pearson coefficient (r), were analyzed using four rainfall intensity thresholds (I in mm/day) based on the World Meteorological Organization (WMO) (2014), considering an additional class, due to the sensibility of the SRE's. The classification of the intensity of the rainfall used was light (1 mm/day < I < 2.5 mm/day), moderate (2.5 mm/day < I < 10 mm/day), heavy (10 mm/day < I < 50 mm/day) and violent (I > 50 mm/day). The performance of both sensors based on

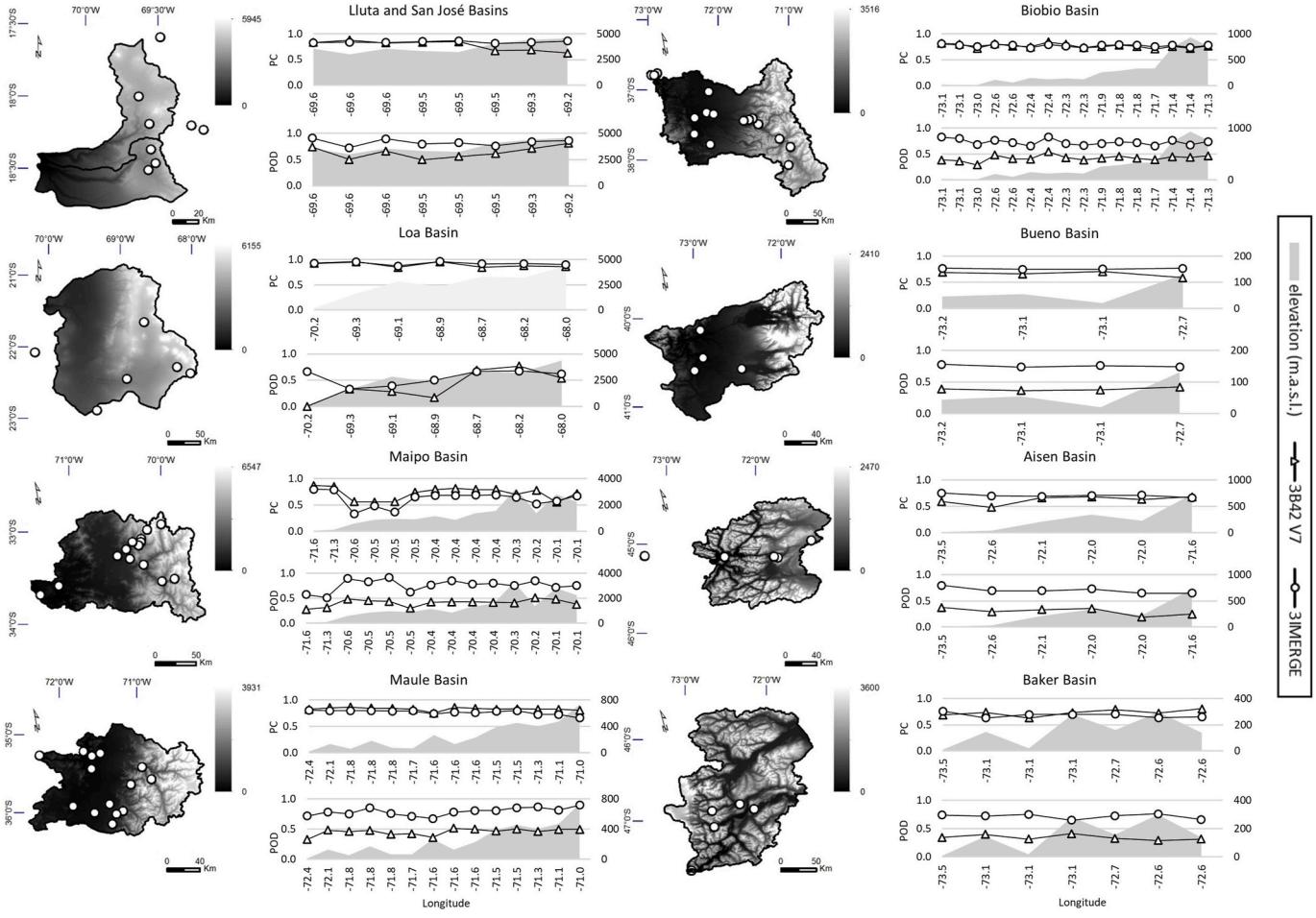

Fig. 4. Performance based on PC and POD indicators for each SER's in each of the defined basins.

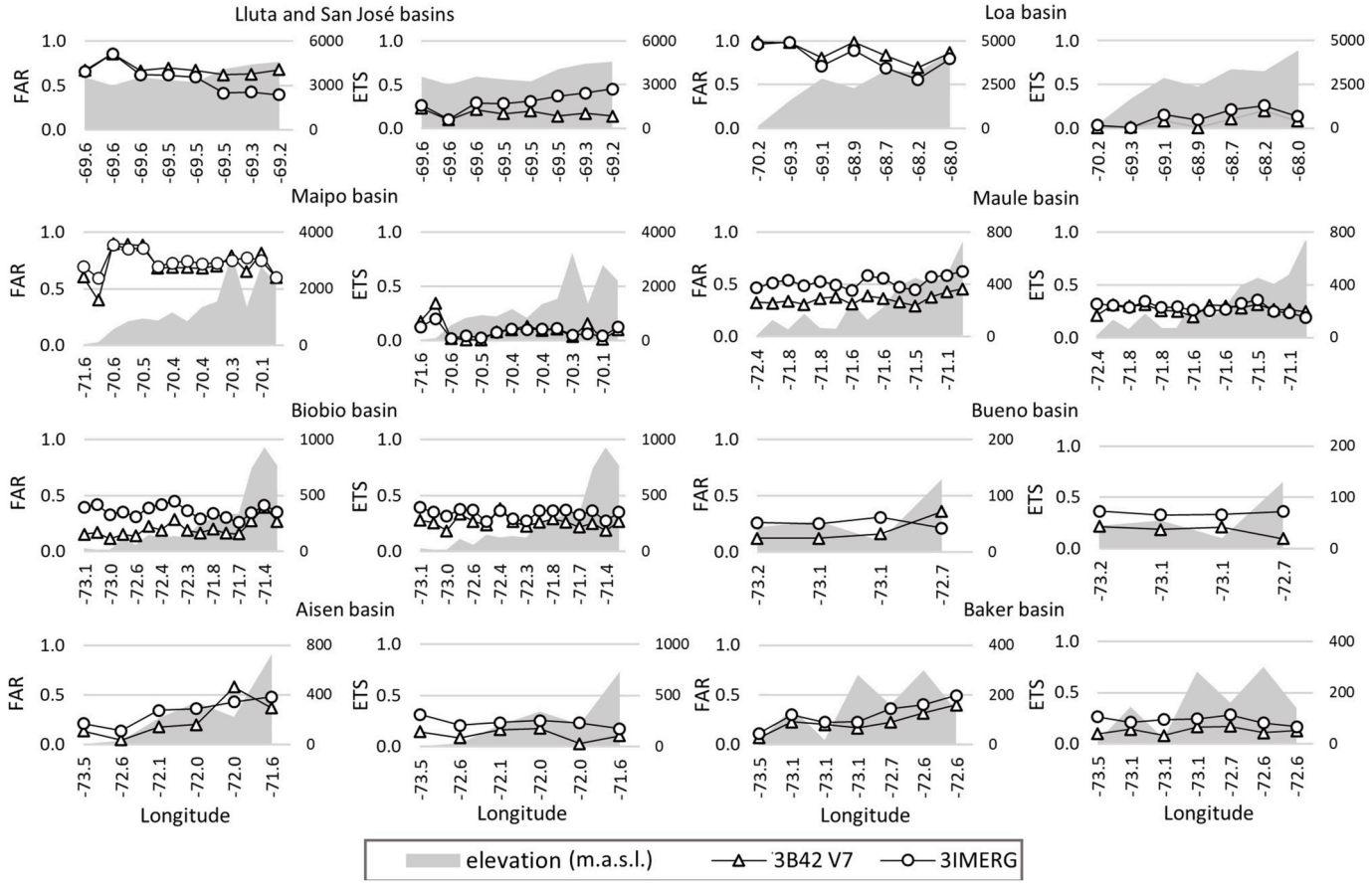

Fig. 5. Results of FAR and ETS indices for the meteorological stations in the basin analyzed.

the r coefficient is shown in Fig. 6, through a box-and-whisker plot.

From Fig. 6, it is possible to verify that the average correlation values have little significance, close to a null correlation (r = 0). Furthermore, for both SRE's, these values do not present a large dispersion, except for rainfalls where I > 50 mm, in this case the value of the r indicator also improves (only 3% of the total events analyzed were over this range). In general, the 3IMERG product has better results than the 3B42 V7. In the Central, South and Austral macro zones, r presents a smaller dispersion

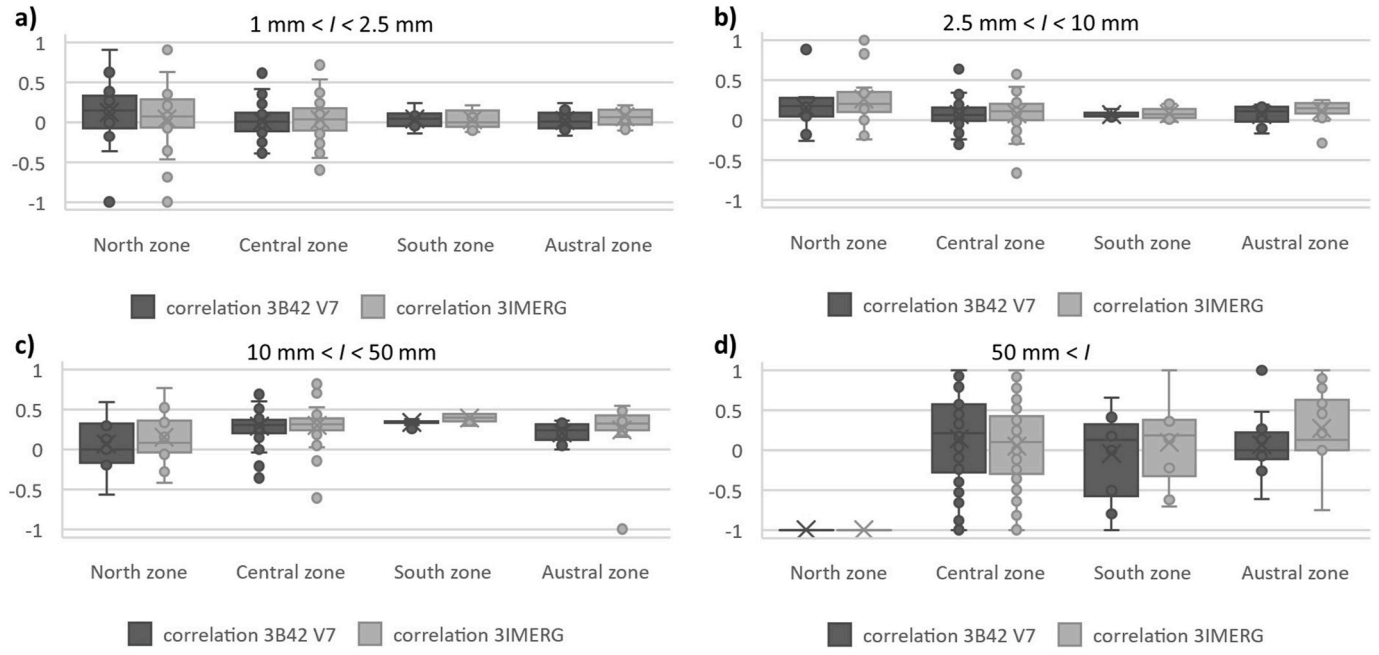

Fig. 6. Results for the linear Pearson coefficient r to comparing the data from SRE's and the meteorological stations, in each macro zone according to the WMO intensity rainfall classification. The boxes are containing the first and third quartile.

with respect to the average (Fig. 6b–d), the largest quantity of rain events with intensity thresholds between 10 and 50 mm/day are concentrated in these macro zones. In the Central macro zone, it stands out that for precipitations with intensity between 1 and 2.5 mm/day (Fig. 3a), the 3B42 V7 products surpasses the performance of the 3IMERG (with average values of r = 0.13 and r = 0.04, respectively). Likewise, for an intensity greater than 50 mm/day (Fig. 3d), the product 3B42 V7 reaches an average value of r = 0.15, while the 3IMERG an r = 0.05.

The BIAS index was calculated for all storms during the period under study, using both estimated rainfall depth (SRE's) and measured rainfall depth (meteorological stations). The results are presented in Fig. 7, where the rainfall depth from 3IMERG were closer to the observed rainfall depth (BIAS close to 1) than the rainfall depth from 3B42 V7. The best performance for the 3IMERG was obtained in the South macro zone with a BIAS mean of 1.08. The best performance of the 3B42 V7 was in the Austral macro zone with a BIAS mean of 0.27. In the Central macro zone (Fig. 7b) the product 3IMERG is able to maintain a good performance with a BIAS mean of 0.87, while in the same macro zone the 3B42 V7 obtains a low performance with a BIAS mean of 0.22.

In the North and Austral zones the precipitations are underestimated (BIAS<1), for both the 3IMERG and the 3B42 V7. The BIAS mean in these two macro zones for the 3IMERG are of 0.64 and 0.76, respectively. For the same zones (North and Austral), the 3B42 V7 has BIAS means of 0.24 and 0.27. Finally, in the Austral macro zone it was observed that for both sensors the BIAS are smaller (there is a larger underestimation of rainfall), except for the O'Higgins station located in the O'Higgins glacier (the Chilean Field Ice, Patagonia), where BIAS>1.

The results for the analysis of the KGE' performance indicator for the entire study area are presented in Fig. 8. The results show that in the vast majority of cases the 3IMERG obtains a better performance compared to its predecessor 3B42 V7.

The best results for the KGE′ are observed in the Central macro zone, where the 3IMERG presents a maximum KGE′ of 0.74, much higher than the 3B42 V7 that obtains a maximum KGE′ of 0.32. In this macro zone the average KGE's of the 3IMERG and 3B42 V7 are of 0.50–0.04 respectively. In the North macro zone, where the stations located at the highest altitude (3000 m.a.s.l) are concentrated, the 3IMERG obtains an average KGE′ of 0.32, with maximum values that are above 0.5. On the other hand, in this same macro zone, 3B42 V7 only reaches an average KGE′ close to 0, whose maximum values are under the threshold of 0.21. In the South and Austral macro zones a decrease in the average performance of the 3B42 V7 (average KGE′ of −0.16 and 0.20, respectively) is observed. In the Austral zone it stands out that the average performance of the 3IMERG is less, with an average KGE′ of 0.28.

Additionally, the storms were analyzed according to the ranges of precipitation intensity and the results for the KGE′ are presented for four basins representative for each macro zone (Fig. 9). In the Lluta and San José basins (North macro zone) the performance of the 3B42 V7 and 3IMERG are similarly bad. The best results for the North macro zone are obtained for the range of precipitation intensity between 10 and 50 mm/day. For the basins of the Central macro zone the results show a better performance for the 3IMERG product maintaining the highest KGE′ values for the range of intensity between 10 and 50 mm/day and the lowest for the intensity range between 1.0 and 2.5 mm/day. In the case of the basins of the South macro zone the 3IMERG obtains the best performance with a maximum KGE′ of 0.14 for precipitations of high intensity (I > 50 mm/day). However, for these same basins (South macro zone), the best result for 3B42 V7 is obtained for the intensity range between 10 and 50 mm/day with a maximum KGE' of −0.62.

4. Analysis and discussion

In general terms, the performances obtained by the 3IMERG product surpasses the 3B42 V7 product, this corresponds to the advances in the equipment used in the precipitation estimates. The higher temporal and spatial resolution of the 3IMERG product results in an improvement in the measurement of precipitations when these are of the cyclonic type (also when these have an orographic component; i.e the cases of Central macro zone) and convective (i.e the case of the North macro zone), of short duration and spatially little extended. Similar results, on the improvement of 3IMERG estimations for short-term events were found by Tan and Duan (2017) and Xu et al. (2017). The better capacity of the 3IMERG is explained by the increase in the frequency band range of the DPR (passing from 13.60 GHz in the TRMM to 35.55 GHz in the GPM). In addition, the greater quantity of channels included in the GMI sensor provides a better estimation and sensibility to events of a lower intensity (>0.5 mm) and for a shorter period of time (0.5hr), including the

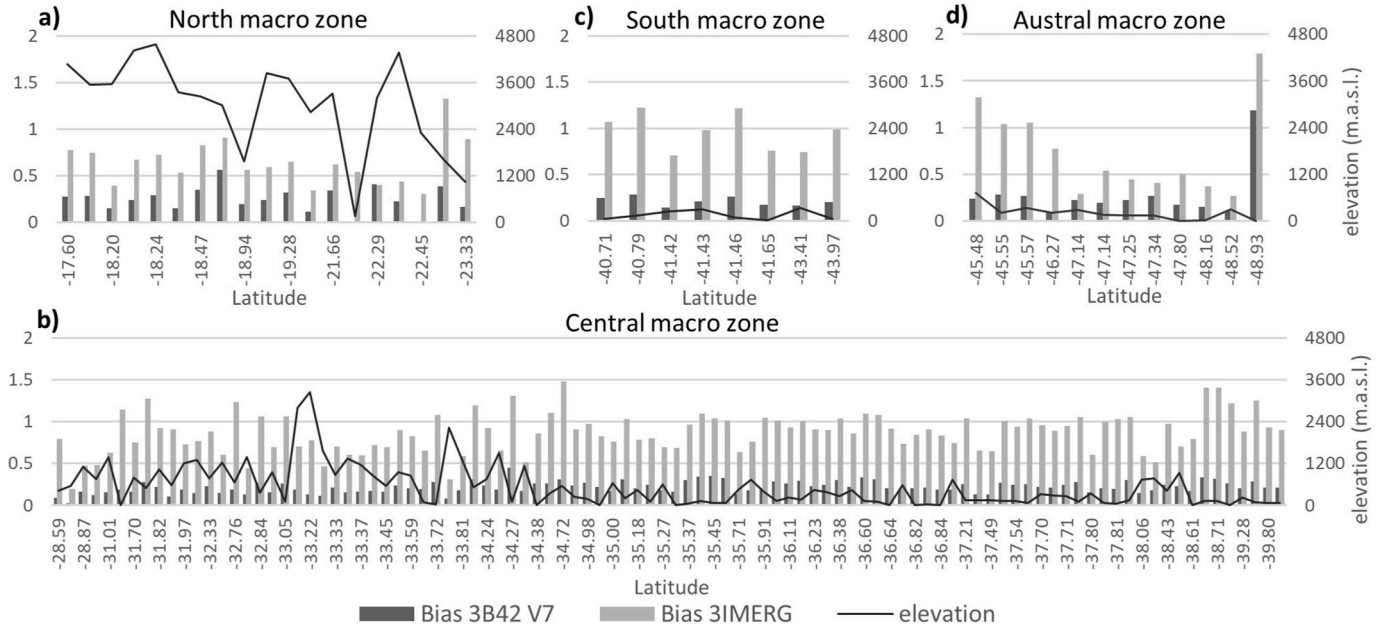

Fig. 7. Results for BIAS of 3IMERG and 3B42 V7 for the macro zones SRE's a) North, b) Central, c) South and d) Austral. The secondary axe represents the elevation of the meteorological stations.

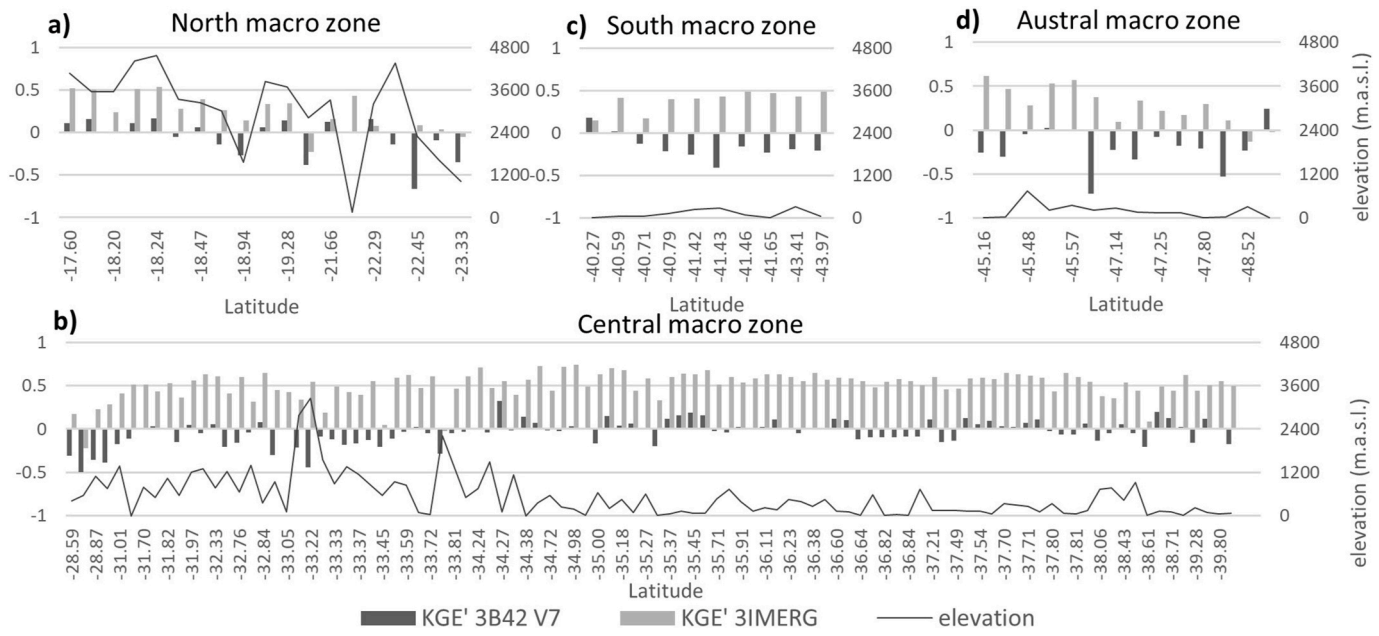

Fig. 8. Results for KGE′ for both SRE's in each macro zone. The secondary axe represents the elevation of the meteorological stations.

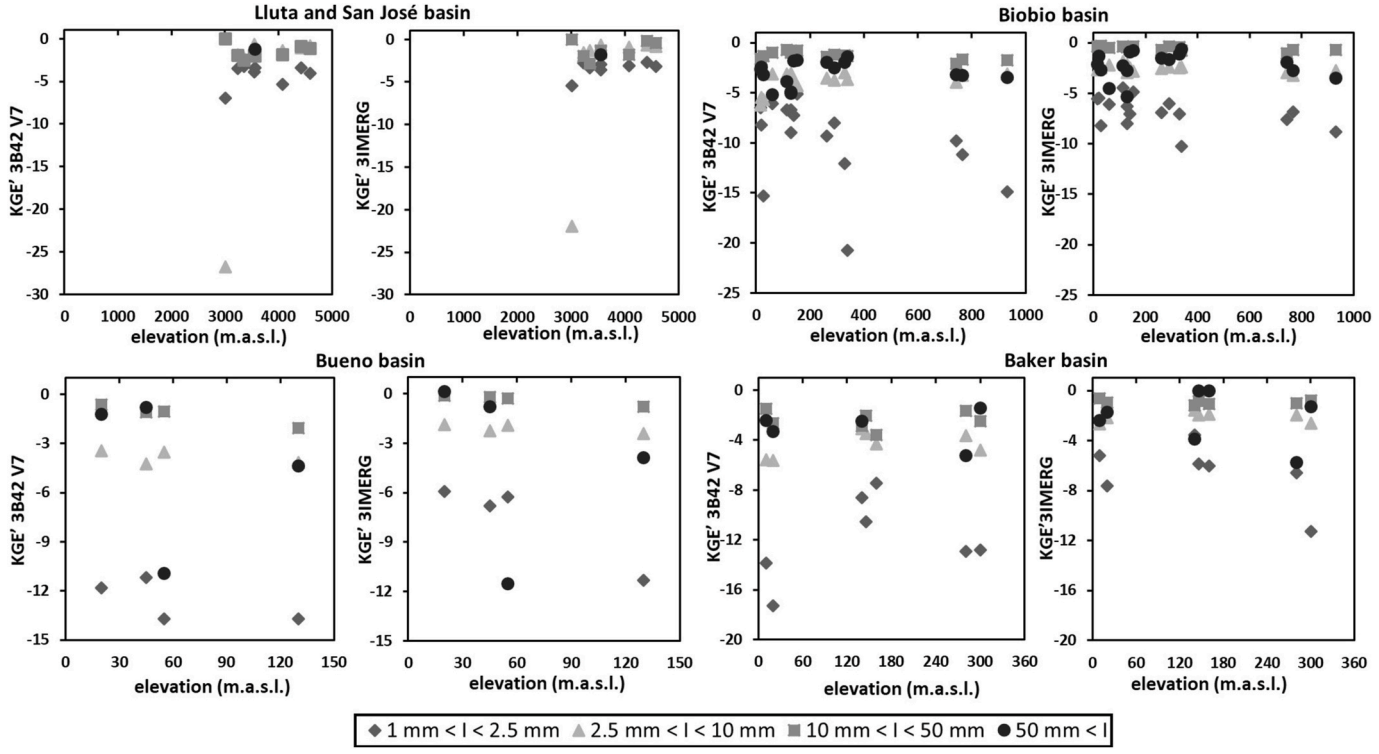

Fig. 9. Graphics of the KGE′ results for four basins, each which correspond to a different macro zone. The results are shown in different tones for each precipitation threshold.

identification of ice particles (JAXA, 2018). The intensity of the precipitation is a factor that influences the performance of the SRE's, the best indicator values for both the categories (Fig. 6) and the statistics (Fig. 9), are obtained for the heavy events (10–50 mm/day) and violent events (>50 mm/day).

The results found in this study are consistent with those obtained by other studies conducted in this area and in other parts of the world. As seen in Fig. 3, there is an improvement in the performance of the SRE's between the dry and wet seasons, this is a tendency that is repeated in other parts of the world such as Pakistan (Hussain et al., 2018) and Brazil (Salles et al., 2019). Zambrano-Bigiarini et al. (2017), for the different macro zones of Chile, found that the TRMM (product 3B42 V7) has better results than other SER's (ex. CMORPH, PERSIANN). On the other hand, Mendez Rivas (2016), for the Central macro zone of Chile, obtained better performances with the 3IMERG product than with the 3B42 V7 (both in the identification of events as well as with the estimation of rainfall volume).

The hyper-arid characteristics of the North macro zone condition the

ability of the sensors for the correct identification and quantification of the precipitation. In this same macro zone, the value of the PC index during dry seasons (autumn, winter and spring) is greater (see Fig. 3). The previous is explained due to during this dry period there are less hits (H) and a greater quantity of correct negative (CN). In the coastal areas and inland valleys of the North macro zone (<3000 m.a.s.l), the POD has a lower value (for the 3IMERG and 3B42 V7 products the average POD is 0.53 and 0.29 respectively) than in the *Altiplano* (*Andes Mountain Range*; average POD of 0.82 for the 3IMERG product and 0.71 for the 3B42 V7 product). This difference in the POD indicator can be explained because these areas (coastal and inland valleys) have frequently high cloudiness (Cereceda and Schemenauer, 1991) but very little precipitation.

In the Central macro zone the best results were observed for the low altitude zones (<1000 m.a.s.l). The values of the categorical indices obtain the worse results in the medium elevation (1000–2000 m.a.s.l) and high elevation (>2000 m.a.s.l) zones. The 3IMERG product obtains POD values above the 3B42 V7 in the entire Central macro zone (the mean values for 3IMERG and 3B42 V7 were 0.85 and 0.51, respectively). On the other hand, the FAR indicator showed that the 3IMERG product (mean FAR of 0.66) obtained a greater quantity of false alarms (FA), in comparison with the 3B42 V7 product (mean FAR of 0.53). Considering the POD and FAR indicator results, the 3IMERG has a high probability to detect rainfall events, but it can also generate a large quantity of false alarms.

In the South and Austral macro zones the 3IMERG product maintains a superiority in the identification of rain events with respect to the 3B42 V7 product. The mean POD for the 3IMERG is 0.84 and 0.81 in the South and Austral macro zones, respectively and the mean POD for the 3B42 V7 product is 0.73 (for both macro zones).

As in the Central macro zone, the FAR index showed that the 3IMERG product delivers a greater quantity of FA, compared to the 3B42 V7 (the 3IMERG product obtains an average FAR of 0.36 and 0.53, while the 3B42 V7 product an average FAR of 0.23 and 0.41, for the South and Austral macro zones, respectively). For these two macro zones the stations are located at a low elevation (0–1000 m.a.s.l), thus, these are influenced by cold masses and rainfall of the frontal type in the wettest seasons (mainly during winter) (Barrett and Hameed, 2017).

Considering the results found for the detection rates for high-elevation locations in the central macro zone, and for locations where permanent ice and snow climates are met in the south and austral macro zones, one of the difficulties for SRE's lies in the distinction between liquid and solid precipitation. Hussain et al. (2018), points out that for mountainous, and glacial areas, the presence of cold clouds and ice fields makes SRE's estimates difficult due to the fact that the temperature threshold of the clouds to discriminate snow and rain precipitation is difficult to determine. As a consequence, clouds that have temperatures above this threshold can be mistakenly identified as rain when they are not. In line with the above, for the stations located in the high-elevation zones (above 2000 m.a.s.l) the results of the products are conditioned by climatic and topographic factors (see Table 2).

From Table 2 it can be seen that the PC index for the 3IMERG is lower than the product 3B42 V7 at low and medium elevations. At high elevations the 3IMERG has a better percentage of correct identifications compared with the 3B42 V7.

For the POD index, the 3IMERG maintains a better ability to identify rainfall events with respect to 3B42 V7 over entire range of elevations, but this index decrease its effectiveness in identifying events at higher altitude locations.

Both products 3IMERG and 3B42 V7 have a higher FAR index at high elevations. At high elevations, the product 3IMERG has lower FA values than the 3B42 V7.

The ETS index shows no differences at low and medium elevations, while for high elevations the differences between 3IMERG and 3B42 V7 is greater (See Table 2).

The continuous statistical indices demonstrated that the quantification of rainfall depth in the case of both products is bad/poor.

Table 2
Mean values for categorical and continuous indices for all the stations at low (0–1000 m.a.s.l.), medium (1000–2000 m.a.s.l.) and high (2000 m.a.s.l. <) elevations.

	Elevation (m.a.s.l.)		
	0-1000 (3IMERG; 3B42 V7)	1000-2000 (3IMERG; 3B42 V7)	2000< (3IMERG; 3B42 V7)
PC	0.75 ; 0.82	0.74 ; 0.86	0.81 ; 0.78
POD	0.85 ; 0.50	0.78 ; 0.44	0.77 ; 0.61
FAR	0.60 ; 0.46	0.85 ; 0.82	0.78 ; 0.84
ETS	0.25 ; 0.25	0.09 ; 0.10	0.16 ; 0.09
R	0.63 ; 0.55	0.57 ; 0.50	0.55 ; 0.46
BIAS	0.91 ; 0.23	0.67 ; 0.18	0.59 ; 0.24
KGE'	0.48 ; −0.06	0.35 ; −0.12	0.27 ; −0.07

For different rainfall ranges, the Pearson coefficient was calculated (Fig. 6.) and it was found that SRE's quantify better rainfall for heavy precipitations (10 mm/day < I < 50 mm/day). For the South macro zone (where the greatest quantity of rain events are concentrated) the high values of r were found (the 3IMERG product obtained an r = 0/39 and the 3B42 V7 product an r = 0.34).

The results for the BIAS index obtained in the Central macro zones (mean BIAS of 0.86) and South macro zone (mean BIAS of 0.21) are consistent with previous studies conducted in these macro zones (Mendez Rivas, 2016; Baez-Villanueva et al., 2018; and Rivera et al., 2018), where the SRE's underestimate the precipitation amounts. The presence of the Coastal Mountain Range and of the Andes Mountain Range in the generation and distribution of precipitation (Viale and Nuñez, 2010; Garreaud et al., 2016) is an important factor in the results obtained in this study. These results are similar to those described by (Asong et al. (2017) in the area of the Rocky Mountains (Canada) and Caracciolo et al. (2018) in the islands of Sicily and Sardinia, where the 3IMERG had underestimations. In these two areas the influence of the maritime climate and the influence of orographic effects is very relevant.

All the stations at high elevations (above 2000 m.a.s.l) are concentrated in the North and Central macro zones where the BIAS values tend to underestimate the rainfall (mean BIAS of 0.59 for 3IMERG and 0.24 for 3B42 V7). This underestimation is produced because of the Andes Mountains where the air masses rise rapidly, cool and produce condensation in a short period of time, increasing the amount of rainfall that SRE's fail to capture.

The frontal systems moved because of the pacific anticyclone and the low temperatures in the Austral condition the snow fall, including in areas located at low elevations. In this macro zone it was found that both SRE's overestimate the rain amounts (BIAS > 1), in the Glacier O'Higgins station (48°S), whose BIAS was 1.79 and BIAS = 1.18 for the 3IMERG and 3B42 V7, respectively. As indicated by Bharti and Singh (2015), the overestimation of rain by the SRE's typically occures in areas where ice fields exist and there is a presence of clouds made up of solid water particles (cirrus clouds), these are the conditions that can be found in the Glacier O'Higgins station.

5. Conclusions

The evaluation carried out in this paper evidenced that despite the technological advances in the SRE's, not minor uncertainties still exist in the products of TMPA and GPM satellite mission. The analysis conducted across the 3600 km of the Chilean territory shows that the most important factors that affect the rainfall estimation are: i) the hydroclimatic characteristics of the zone, ii) the season being evaluated (wet/dry) and iii) the relief (topography). The results at a general level show that the 3IMERG product of IMERG and the 3B42 V7 product of TMPA are not able to capture satisfactorily the rain events in the different macro zones analyzed. Some exceptions, where the rainfall amounts are estimated with a greater level of precision by the SRE's, occur in hydroclimatic zones that present high intensity rain and were the orographic effect is less marked (certain areas of the Central and South macro zones). Additionally, it was observed that the 3IMERG product, with respect to its predecessor 3B42 V7, obtains better results in the ability to identify and estimate rainfall.

With the performance comparison of the 3IMERG and 3B42 V7 products in the different macro hydroclimatic zones the following conclusions can be made:

- Both SRE's obtained their best PC results in the dry seasons, while for the POD, FAR, and ETS the best results were obtained in the wet seasons. In the North macro zone, the POD, FAR and ETA indices were at the highest in summer (Altiplano winter corresponding to the wet season), while the best values in the rest of the macro zones (Central, South and Austral) were obtained during the autumn and winter months (wet season).
- Through the Pearson r correlation analysis, it was obtained that for precipitations of intensities in the range of 10–50 mm/day, the SRE's improve their identification and estimation of rain events. According to the BIAS analysis, the estimations of the 3IMERG product for all the zones studied, are more precise than the 3B42 V7 product. These results can support the analysis of flood and water balances in the areas with low season density (ex: macro North zone).
- Regarding the temporal and volumetric dynamics of the rain events analyzed, using the KGE index, it was confirmed that the 3IMERG is capable of obtain better results than the 3B42 V7.
- In areas of high elevation gradient, precipitation events are more difficult to detect and quantify, both because of the rapid rise of air masses and their condensation, as well as the distinction between liquid and solid precipitation. Under these conditions, the identification and quantification of rainfall depth in the *Coastal Mountain Range* and *Andes Mountain Range* (where the rainfall events are mainly cyclonic and sometimes with an orographic forcing) by 3IMERG is better than 3B42 V7.

It can be concluded that the 3IMERG product has greatly surpassed its predecessor 3B42 V7. A future challenge for the remote precipitation sensors corresponds to the use in zones where the elevation gradients are an important factor in the generation of precipitation. It is necessary to see the implications of the type of precipitation in the results to have an improvement in the calibration of the algorithms that generate these products, nevertheless, the lack of information measured in the field (temporal and spatial gaps) makes this task difficult. The 3IMERG product could be a strong source of data for studies that impact that climatic disturbances have on the hydrologic cycles in the Central and South zones of Chile. Additionally, its usefulness is fundamental in remote zones or in areas where access is complicated for the obtainment of data where it is difficult to install stations. This is the case of the altiplano zone of the north, a place where there are also events of a convective nature (especially not widespread) and in zones with complicated access like part of the Chilean Andes.

Finally, this product provides the possibility to feed rain-runoff models, for the study of floods, widening the spatial information of the seasons of the land. Given the climatic and geographical diversity of Chile, this study can help to evaluate the performance of the 3IMERG and 3B42 V7 products for other zones of the planet with hydroclimatic similarities.

CRediT authorship contribution statement

Marco Soto-Alvarez: Investigation, Formal analysis. **Hernán Alcayaga:** Conceptualization, Supervision. **Vladimir Alarcon:** Writing - original draft. **Diego Caamaño:** Writing - review & editing. **Sebastián Palma:** Methodology. **Rossana Escanilla:** Methodology.

Declaration of competing interest

The authors declare that they have no known competing financial interests or personal relationships that could have appeared to influence the work reported in this paper.

References

Alarcon, V.J., Alcayaga, H., Alvarez, E., 2015. Assimilation of TRMM precipitation into a hydrological model of a southern Andes watershed. https://doi.org/10.1007/978-3-319-21470-2_34, 468 476.

Asong, Z.E., Razavi, S., Wheater, H.S., Wong, J.S., 2017. Evaluation of integrated multisatellite retrievals for GPM (IMERG) over southern Canada against ground precipitation observations: a preliminary assessment. J. Hydrometeorol. 18, 1033–1050. https://doi.org/10.1175/jhm-d-16-0187.1.

Baez-Villanueva, O.M., Zambrano-Bigiarini, M., Ribbe, L., Nauditt, A., Giraldo-Osorio, J. D., Thinh, N.X., 2018. Temporal and spatial evaluation of satellite rainfall estimates over different regions in Latin-America. Atmos. Res. 213, 34–50. https://doi.org/10.1016/j.atmosres.2018.05.011.

Barrett, B.S., Hameed, S., 2017. Seasonal variability in precipitation in central and southern Chile: modulation by the south pacific high. J. Clim. 30, 55–69. https://doi.org/10.1175/JCLI-D-16-0019.1.

Bharti, V., Singh, C., 2015. Evaluation of error in TRMM 3B42V7 precipitation estimates over the Himalayan region. J. Geophys. Res. Atmos. 120, 12458–12473. https://doi.org/10.1002/2015JD023779.

Blöschl, G., Bierkens, M.F.P., Chambel, A., Cudennec, C., Destouni, G., Fiori, A., Kirchner, J.W., McDonnell, J.J., Savenije, H.H.G., Sivapalan, M., Stumpp, C., Toth, E., Volpi, E., Carr, G., Lupton, C., Salinas, J., Széles, B., Viglione, A., Aksoy, H., Allen, S.T., Amin, A., Andréassian, V., Arheimer, B., Aryal, S.K., Baker, V., Bardsley, E., Barendrecht, M.H., Bartosova, A., Batelaan, O., Berghuijs, W.R., Beven, K., Blume, T., Bogaard, T., Borges de Amorim, P., Böttcher, M.E., Boulet, G., Breinl, K., Brilly, M., Brocca, L., Buytaert, W., Castellarin, A., Castelletti, A., Chen, X., Chen, Yangbo, Chen, Yuanfang, Chifflard, P., Claps, P., Clark, M.P., Collins, A.L., Croke, B., Dathe, A., David, P.C., de Barros, F.P.J., de Rooij, G., Di Baldassarre, G., Driscoll, J.M., Duethmann, D., Dwivedi, R., Eris, E., Farmer, W.H., Feiccabrino, J., Ferguson, G., Ferrari, E., Ferraris, S., Fersch, B., Finger, D., Foglia, L., Fowler, K., Gartsman, B., Gascoin, S., Gaume, E., Gelfan, A., Geris, J., Gharari, S., Gleeson, T., Glendell, M., Gonzalez Bevacqua, A., González-Dugo, M.P., Grimaldi, S., Gupta, A.B., Guse, B., Han, D., Hannah, D., Harpold, A., Haun, S., Heal, K., Helfricht, K., Herrnegger, M., Hipsey, M., Hlaváčiková, H., Hohmann, C., Holko, L., Hopkinson, C., Hrachowitz, M., Illangasekare, T.H., Inam, A., Innocente, C., Istanbulluoglu, E., Jarihani, B., Kalantari, Z., Kalvans, A., Khanal, S., Khatami, S., Kiesel, J., Kirkby, M., Knoben, W., Kochanek, K., Kohnová, S., Kolechkina, A., Krause, S., Kreamer, D., Kreibich, H., Kunstmann, H., Lange, H., Liberato, M.L.R., Lindquist, E., Link, T., Liu, J., Loucks, D.P., Luce, C., Mahé, G., Makarieva, O., Malard, J., Mashtayeva, S., Maskey, S., Mas-Pla, J., Mavrova-Guirguinova, M., Mazzoleni, M., Mernild, S., Misstear, B.D., Montanari, A., Müller-Thomy, H., Nabizadeh, A., Nardi, F., Neale, C., Nesterova, N., Nurtaev, B., Odongo, V.O., Panda, S., Pande, S., Pang, Z., Papacharalampous, G., Perrin, C., Pfister, L., Pimentel, R., Polo, M.J., Post, D., Prieto Sierra, C., Ramos, M.H., Renner, M., Reynolds, J.E., Ridolfi, E., Rigon, R., Riva, M., Robertson, D.E., Rosso, R., Roy, T., Sá, J.H.M., Salvadori, G., Sandells, M., Schaefli, B., Schumann, A., Scolobig, A., Seibert, J., Servat, E., Shafiei, M., Sharma, A., Sidibe, M., Sidle, R.C., Skaugen, T., Smith, H., Spiessl, S.M., Stein, L., Steinsland, I., Strasser, U., Su, B., Szolgay, J., Tarboton, D., Tauro, F., Thirel, G., Tian, F., Tong, R., Tussupova, K., Tyralis, H., Uijlenhoet, R., van Beek, R., van der Ent, R.J., van der Ploeg, M., Van Loon, A.F., van Meerveld, I., van Nooijen, R., van Oel, P.R., Vidal, J.P., von Freyberg, J., Vorogushyn, S., Wachniew, P., Wade, A.J., Ward, P., Westerberg, I.K., White, C., Wood, E.F., Woods, R., Xu, Z., Yilmaz, K.K., Zhang, Y., 2019. Twenty-three unsolved problems in hydrology (UPH)–a community perspective. Hydrol. Sci. J. 64, 1141–1158. https://doi.org/10.1080/02626667.2019.1620507.

Cabrera, J., Yupanqui, R.T., Rau, P., 2016. Validation of TRMM daily precipitation data for extreme events analysis. The case of piura watershed in Peru. Procedia Eng 154, 154–157. https://doi.org/10.1016/j.proeng.2016.07.436.

Cao, Y., Zhang, W., Wang, W., 2018. Evaluation of TRMM 3B43 data over the Yangtze river delta of China. Sci. Rep. 8, 5290. https://doi.org/10.1038/s41598-018-23603-z.

Caracciolo, D., Francipane, A., Viola, F., Noto, L.V., Deidda, R., 2018. Performances of GPM satellite precipitation over the two major Mediterranean islands. Atmos. Res. 213, 309–322. https://doi.org/10.1016/j.atmosres.2018.06.010.

Cereceda, P., Schemenauer, R.S., 1991. The occurrence of fog in Chile. J. Appl. Meteorol. 30, 1097–1105. https://doi.org/10.1175/1520-0450(1991)030<1097:TOOFIC>2.0.CO;2.

Demaria, E.M.C., Maurer, E.P., Thrasher, B., Vicuña, S., Meza, F.J., 2013. Climate change impacts on an alpine watershed in Chile: do new model projections change the story? J. Hydrol. 502, 128–138. https://doi.org/10.1016/j.jhydrol.2013.08.027.

Dinku, T., Ceccato, P., Grover-Kopec, E., Lemma, M., Connor, S.J., Ropelewski, C.F., 2007. Validation of satellite rainfall products over East Africa's complex topography. Int. J. Rem. Sens. 28, 1503–1526. https://doi.org/10.1080/01431160600954688.

Dinku, T., Chidzambwa, S., Ceccato, P., Connor, S.J., Ropelewski, C.F., 2008. Validation of high-resolution satellite rainfall products over complex terrain. Int. J. Rem. Sens. 29, 4097–4110. https://doi.org/10.1080/01431160701772526.

Garreaud, R., Falvey, M., Montecinos, A., 2016. Orographic precipitation in coastal southern Chile: mean distribution, temporal variability, and linear contribution. J. Hydrometeorol. 17, 1185–1202. https://doi.org/10.1175/JHM-D-15-0170.1.

Gunn, J., 2004. Encyclopedia of caves and karst science. In: Gunn, J. (Ed.), Fitzroy Dearborn.

Gupta, H.V., Kling, H., Yilmaz, K.K., Martinez, G.F., 2009. Decomposition of the mean squared error and NSE performance criteria: implications for improving hydrological modelling. J. Hydrol. 377, 80–91. https://doi.org/10.1016/j.jhydrol.2009.08.003.

Hobouchian, M.P., Salio, P., García Skabar, Y., Vila, D., Garreaud, R., 2017. Assessment of satellite precipitation estimates over the slopes of the subtropical Andes. Atmos. Res. 190, 43–54. https://doi.org/10.1016/j.atmosres.2017.02.006.

Houston, J., 2006. Variability of precipitation in the Atacama Desert: its causes and hydrological impact. Int. J. Climatol. 26, 2181–2198. https://doi.org/10.1002/joc.1359.

Huffman, G.J., 2016. The Transition in Multi-Satellite Products from TRMM to GPM (TMPA to IMERG).

Huffman, G.J., Adler, R.F., Bolvin, D.T., Nelkin, E.J., 2010. Satellite rainfall applications for surface hydrology. In: Gebremichael, M., Hossain, F. (Eds.), Satellite Rainfall Applications for Surface Hydrology. Springer Netherlands, Dordrecht, pp. 3–22. https://doi.org/10.1007/978-90-481-2915-7.

Huffman, G.J., Bolvin, D.T., Nelkin, E.J., 2017. Integrated Multi-satellitE Retrievals for GPM (IMERG) Technical Documentation.

Huffman, G.J., Bolvin, D.T., Nelkin, E.J., Wolff, D.B., Adler, R.F., Gu, G., Hong, Y., Bowman, K.P., Stocker, E.F., 2007. The TRMM multisatellite precipitation analysis (TMPA): quasi-global, multiyear, combined-sensor precipitation estimates at fine scales. J. Hydrometeorol. 8, 38–55. https://doi.org/10.1175/JHM560.1.

Hussain, Y., Satgé, F., Hussain, M.B., Martinez-Carvajal, H., Bonnet, M.P., Cárdenas-Soto, M., Roig, H.L., Akhter, G., 2018. Performance of CMORPH, TMPA, and PERSIANN rainfall datasets over plain, mountainous, and glacial regions of Pakistan. Theor. Appl. Climatol. 131, 1119–1132. https://doi.org/10.1007/s00704-016-2027-z.

Insel, N., Poulsen, C.J., Ehlers, T.A., 2010. Influence of the Andes Mountains on South American moisture transport, convection, and precipitation. Clim. Dynam. 35, 1477–1492. https://doi.org/10.1007/s00382-009-0637-1.

JAXA, 2018. GPM Data Utilization Handbook, 3.1.

Kidd, C., Levizzani, V., 2011. Status of satellite precipitation retrievals. Hydrol. Earth Syst. Sci. 15, 1109–1116. https://doi.org/10.5194/hess-15-1109-2011.

Kling, H., Fuchs, M., Paulin, M., 2012. Runoff conditions in the upper Danube basin under an ensemble of climate change scenarios. J. Hydrol. 424–425, 264–277. https://doi.org/10.1016/j.jhydrol.2012.01.011.

Mantas, V.M., Liu, Z., Caro, C., Pereira, A.J.S.C., et al., 2014. Validation of TRMM multi-satellite precipitation analysis (TMPA) products in the Peruvian Andes. Atmos. Res. 163 https://doi.org/10.1016/j.atmosres.2014.11.012. In press.

McPhee, J., 2018. Water Policy in Chile, Water Policy in Chile, Global Issues in Water Policy. Springer International Publishing, Cham. https://doi.org/10.1007/978-3-319-76702-4.

Mendez Rivas, R.A., 2016. Productos de precipitacion satelital de alta resolucion espacial y temporal en zonas de topografia compleja. Pontificia Universidad Catolica de Chile.

OECD, 2018. OECD Economic Surveys: Chile 2018, OECD Economic Surveys: Chile. OECD Publishing, Paris. https://doi.org/10.1787/eco_surveys-chl-2018-en.

Rivera, J.A., Marianetti, G., Hinrichs, S., 2018. Validation of CHIRPS precipitation dataset along the central Andes of Argentina. Atmos. Res. 213, 437–449. https://doi.org/10.1016/j.atmosres.2018.06.023.

Salles, L., Satgé, F., Roig, H., Almeida, T., Olivetti, D., Ferreira, W., 2019. Seasonal effect on spatial and temporal consistency of the new GPM-based IMERG-v5 and GSMaP-v7 satellite precipitation estimates in Brazil's central plateau region. Water 11, 668. https://doi.org/10.3390/w11040668.

Sharifi, E., Steinacker, R., Saghafian, B., 2016. Assessment of GPM-IMERG and other precipitation products against gauge data under different topographic and climatic conditions in Iran: preliminary results. Rem. Sens. 8 https://doi.org/10.3390/rs8020135.

Tan, M.L., Duan, Z., 2017. Assessment of GPM and TRMM precipitation products over Singapore. Rem. Sens. 9, 1–16. https://doi.org/10.3390/rs9070720.

Tan, M.L., Santo, H., 2018. Comparison of GPM IMERG, TMPA 3B42 and PERSIANN-CDR satellite precipitation products over Malaysia. Atmos. Res. 202, 63–76. https://doi.org/10.1016/j.atmosres.2017.11.006.

Tarek, M.H., Hassan, A., Bhattacharjee, J., Choudhury, S.H., Badruzzaman, A.B.M., 2017. Assessment of TRMM data for precipitation measurement in Bangladesh. Meteorol. Appl. 24, 349–359. https://doi.org/10.1002/met.1633.

Tian, Y., Peters-Lidard, C.D., Eylander, J.B., Joyce, R.J., Huffman, G.J., Adler, R.F., Hsu, K.L., Turk, F.J., Garcia, M., Zeng, J., 2009. Component analysis of errors in Satellite-based precipitation estimates. J. Geophys. Res. Atmos. 114, 1–15. https://doi.org/10.1029/2009JD011949.

Viale, M., Nuñez, M.N., 2010. Climatology of winter orographic precipitation over the subtropical central Andes and associated synoptic and regional characteristics. J. Hydrometeorol. 12, 481–507. https://doi.org/10.1175/2010jhm1284.1.

Wang, G., Zhang, P., Liang, L., Zhang, S., 2017. Evaluation of precipitation from CMORPH, GPCP-2, TRMM 3B43, GPCC, and ITPCAS with ground-based measurements in the Qinling-Daba Mountains, China. PloS One 12, e0185147. https://doi.org/10.1371/journal.pone.0185147.

World Meteorological Organization (WMO), 2014. Guide to meteorological instruments and methods of observation, 2014 update. In: Guide to Meteorological Instruments and Methods of Observation. World Meteorological Organization (WMO), Geneva.

Xu, R., Tian, F., Yang, L., Hu, H., Lu, H., Hou, A., 2017. Ground validation of GPM IMERG and TRMM 3B42V7 rainfall products over Southern Tibetan plateau based on a high-density rain gauge network. J. Geophys. Res. 122, 910–924. https://doi.org/10.1002/2016JD025418.

Zad, S.N.M., Zulkafli, Z., Muharram, F.M., 2018. Satellite rainfall (TRMM 3B42-V7) performance assessment and adjustment over Pahang river basin, Malaysia. Rem. Sens. 10, 1–24. https://doi.org/10.3390/rs10030388.

Zambrano-Bigiarini, M., Nauditt, A., Birkel, C., Verbist, K., Ribbe, L., 2017. Temporal and spatial evaluation of satellite-based rainfall estimates across the complex topographical and climatic gradients of Chile. Hydrol. Earth Syst. Sci. 21, 1295–1320. https://doi.org/10.5194/hess-21-1295-2017.